



Research Paper

# Impact of Shape Dependent Ternary Hybrid Nanoliquid Flow through a Microchannel with Quadratic Thermal Radiation: Irreversibility Analysis

B.J. Gireesha<sup>1</sup>, L. Anitha<sup>1,2</sup>

<sup>1</sup> Department of PG Studies and Research in Mathematics, Kuvempu University, Shankaraghatta-577451, Shivamogga, Karnataka, India, Email: bjgireesu@rediffmail.com

<sup>2</sup> Department of Mathematics, Adichunchanagiri Institute of Technology, Chikkamagaluru-577102, Karnataka, India, Email: anitha.l2004@gmail.com

Received December 30 2024; Revised April 14 2024; Accepted for publication April 14 2024.

Corresponding author: B.J. Gireesha (bjgireesu@rediffmail.com)

© 2024 Published by Shahid Chamran University of Ahvaz

**Abstract.** The elite implementations of the trihybrid nanoliquid are converting solar thermal energy, photovoltaic heat collectors, and power storage. This work explores the irreversibility analysis in an upright microchannel subjected to convective ternary hybrid nanoliquid flow with quadratic thermal radiation. The consequences of the Darcy Forchheimer rule, heat source coefficient, and no slip condition on the thermal performance are studied. In the base liquid engine oil, the three distinct types of nanoparticles having different shapes including spherical (Ti), cylindrical (MgO) and platelet (Cu) configurations were considered in this scrutiny. The combined model is used to approach trihybrid and hybrid nanoliquid thermophysical properties. The governing partial differential equation is transferred into the ordinary differential equation by employing dimensionless terms. In the next step to solve the ordinary differential equations, the RKF45 numerical technique is used. The acquired upshots divulge that the improved temperature parameter strongly supports the flow profile. Thermal profile inflates with increased Darcy number. The entropy production shows dual behaviour for the escalated quadratic radiation parameter. With an enhanced darcy number of 400%, the entropy generation rises by 14% in the ternary hybrid nanoliquid circumstances and rises by 11% in the hybrid nanoliquid situation. In addition, when the combination of spherical, cylindrical, and platelet nanoparticles is considered the rate of thermal transfer is greater compared to spherical and cylindrical nanoparticle combinations.

**Keywords:** Quadratic thermal radiation, Darcy-Forchheimer rule, ternary hybrid nanoliquid, entropy generation, no-slip, convective boundary conditions.

## 1. Introduction

In the wake of their immense implications in medicine and physiology, scrutiny of various problems in nanofluidic and microfluidics has been grabbed the interest of many researchers and scientists over the past decade. Furthermore, numerous technological implementations and processes which include analysis of biological and chemical samples, material processing, and micro electromechanical systems have been important to these freshly unfolding areas of research. Yang et al. [1] examined transitory features of electroosmotic flow through a slit channel under the impact of an electric double layer of the channel. Meisel and Ehrhard [2] studied electrically excited flow through a channel by employing an asymptotic model in the existence of electrical double layers for mixing applications. Sbragaglia and Prosperetti [3] inspected efficacious slip characteristics for channel flow with a superhydrophobic surface consisting of solid plane boundary with grooves due to surface tension and made a comparison with existing data. Cho et al. [4] described the mass flow distribution with nonuniform heat flux condition through a microchannel and the results exhibit that the mass flow distribution rate tends to be small in change among channels over a definite magnitude of  $n$ . Kalteh [5] numerically explored the impact of differing nanoparticles on the nanoliquid thermal transfer through a two-dimensional channel and exploration confirmed that less pressure drop is seen in water based nanoliquid than others.

Nanoliquids are being found to have superior thermal properties compared to conventional cooling fluids, making them suitable for use in cooling mechanisms for electronic devices, power plants, and automobiles. Nanoliquids can be used as heat-



transfer liquids in solar thermal systems that generate heat from sunlight. Nanoliquids enhanced thermal properties can improve the efficiency of these systems, resulting in increased energy production and lower costs. Ibanez et al. [6] analysed the entropy production of a nanoliquid flow through a permeable channel along with thermal radiation and hydrodynamic slip and the upshot revealed that minimization entropy production is achieved by the optimized magnitude of Biot number. Sharaf et al. [7] employed Eulerian-Lagrangian technique to numerically discuss the impact of convective thermal transfer and nanoliquid particle migration in a channel and the result depicts that thermophoresis had a vital role in nanoparticle deposition on the channel wall. Moshfegh [8] numerically scrutinized the thermal transfer rate of distinct nanoliquids in the channel in the existence of a partial magnetic field and made a comparison statement between experimental and numerical data of the obtained upshot.

A hybrid nanoliquid is a particular kind of nanoliquid formed by incorporating some sort of nanoparticles into a working fluid that has recently been utilized. To make hybrid nanoliquids, two distinct nanomaterials are suspended in a conventional fluid. Hybrid nanoliquids are extensively used in numerous fields of engineering such as refrigeration industries, spacecraft, biomedical, machining coolant, motor cooling, heat pipe reduction in medicine, and high-performance boats. Sindhu and Gireesha [9] explored the thermal analysis of hybrid nanoliquid in a channel with the impact of nonlinear thermal radiation. Abbasi et al. [10] examined the thermal attributes and entropy production analysis of hybrid nanoliquid flow between two collateral walls with shape features and the outturn illustrated that the copper oxide nanoparticles solid volume fraction enhances the temperature profile. Smrity and Yin [11] evaluated the betterment of PHP performance with hybrid nanoliquid containing metallic and metallic oxide nanoparticles and compared the PHP performance to various working liquids.

Ternary hybrid nanoliquid has attracted many researchers and scientists due to its numerous implementation thermal transfer rates. The thermal conductivity and dynamic viscosities of the ternary hybrid nanoliquid are greater than the nanoliquid and hybrid nanoliquid [12]. The trihybrid nanoliquid contains three different varieties of nanoparticles along with the base fluid. Photovoltaic thermal collectors, solar power, and nuclear safety are the indispensable involvement of trihybrid nanoliquid. Due to its satisfactory outcomes on the thermal performance base liquid collated into hybrid nanoliquid and nanoliquid. In this context, Boroomandpour et al. [13] made a comparative examination of the thermal conductivity of a trihybrid nanoliquid containing multiwall carbon nanotubes and the mono nanoliquid, noteworthy outcome noted that enhanced temperature boosts up the thermal conductivity. Das et al. [14] developed a theoretical model to study the mixed convective fully developed ionic ternary hybrid nanoliquid flow induced by magnetohydrodynamic through an upright channel and the outturn delineated that the magnetic field parameter has a noticeable influence on the stream features. Arif et al. [15] discussed the thermal transfer analysis of couple stress Casson trihybrid nanoliquid flowing in a channel by utilizing various shape features of nanoparticles in blood with pharmaceutical implementations and the upshot revealed that blood-based trihybrid nanoliquid improves the thermal transfer rate. Mohanty et al. [16] investigated the flow and thermal characteristics of a cross-trihybrid water-based nanoliquid over a stretched cylinder. The findings might help in comprehending the effectiveness of ternary hybrid nanoliquids implications for various industries under certain conditions.

Boundary conditions are very important for rectifying problems in computational liquid dynamics. It has primary importance due to its presence in biological and energy innovations such as nuclear power, power generation, missile technology, diesel generators, and photovoltaic systems. The combined impact of temperature jump and slip velocity on the hydrodynamic of magnetohydrodynamic forced convective flow through a horizontal channel was estimated by Hamdan et al. [17] and the outcome revealed that  $Kn$  number significantly affects the skin friction factor. Mozaffari et al. [18] utilized the Lattice Boltzmann technique to simulate convective thermal transfer through a channel under an inclination angle on slip velocity and heat flux and the results noted that the buoyancy forces developed by gravity can change the hydrodynamic attributes of the flow. The significant effects of convective boundary condition and Navier slip on magnetohydrodynamic flow of electrically conducting incompressible Casson liquid flowing through a channel with entropy generation was explored by Venkateswarlu and Bhaskar [19] and the notable outcome revealed that the Casson constraint escalates the skin friction coefficient. Madhu et al. [20] analysed the entropy analysis of Carreau fluid flowing in a channel with convective and no slip conditions.

From the outlook of energy management, it has been instituted that thermal performance processes such as thermal transfer modelling and microscale liquid flow. This implicit that irreversibility which shatters the accessible energy leading to incompetence of thermal design exists. In this context, Ebrahimi et al. [21] looked over entropy generation and heat transfer analysis through a rectangular channel with longitudinal vertex generators and the study concluded that entropy production declines in a rectangular channel when nanoliquid is the working fluid. Ranjit et al. [22] analyzed the flow and thermal attributes for two layered electroosmotic peristaltically pumping flow through a channel with entropy generation. Siva and Jangili [23] deliberated the entropy production analysis in electro osmotic non-Newtonian liquid flow in a microchannel with heat flux and the results showed that the temperature reduces with increased couple stress physical parameter. Anitha and Gireesha [24] studied irreversibility analysis in a convective Jeffrey nanoliquid flowing through a vertical channel with thermal properties by employing the Buongiorno model and the outcome discloses that the Bejan number is greatly supported by Jeffrey nanoliquid than the Newtonian liquid.

The examination of thermal transfer in a permeable media is quite an interesting research area for scientists due to its vital role in engineering and science because of its theoretical and physical importance. It has numerous implementations in engineering industries such as thermal insulation, petroleum reservoirs, thermal energy storage, and heat exchanges. In the context, Hayat et al. [25] scrutinized the significant presence of convective boundary conditions in a carbon nanotube Darcy Forchheimer flow induced by rotating convectively heated disk and upshot revealed that skin friction coefficient magnified for the greater magnitude of nanoparticle volume fraction. The analysis of entropy and temperature distribution in electrokinetically induced flow in a hydrophobic microtube implanted in a Darcy-Forchheimer permeable media was investigated by Misra et al. [26] and the study noticed that increased steric effect greatly affected the electrokinetic velocity which declined noticeably. Jakeer et al. [27] explored the significant impact of the Darcy-Forchheimer rule on electromagnetohydrodynamic trihybrid nanoliquid flowing over a stretching surface with heat flux and the outcome revealed that the thermal profile is escalating for the greater magnitude of Eckert number.



Thermal radiation plays a key role in the technique associated with the thermal engineering. The radiative thermal transfer tends to be more noticeable at high temperature. Its feasible application is incorporated in the design of aircraft, space vehicles, and satellites. In processes like nuclear power plants, gas turbines, gas production, and polymer processes radiation plays a significant role. Recently, Shaw et al. [28] analyzed the thermal transfer and hydrodynamic flow characteristics of cross hybrid nanoliquid flow over a stretched cylinder influenced by quadratic radiation and the results exhibit that escalated Weissenberg number upsurged the fluid motion. Rana et al. [29] investigated the impact of quadratic radiation on the nonlinear thermal buoyancy driven flow of hybrid nanoliquid compounded by MWCNT-MgO/EG nanoparticle at the static point of the revolving sphere. The significant influence of quadratic thermal radiation on three-dimensional stagnation points magnetohydrodynamic multiple slip flow of trihybrid nanoliquid flow over a gyrating disk with slip was deliberated by Gupta and Rana [30] and the upshot divulged that the thermal transfer rate diminished for a greater heat source parameter. Thermal analysis of Darcy-Forchheimer trihybrid nanoliquid flow with quadratic thermal radiation was scrutinized by Chen et al. [31] and the outcome discloses the advantages of trihybrid nanoliquid in enhancing solar radiation usage efficiency.

Quadratic thermal radiation has become one of the most interesting research areas due to its crucial applications in space technology, polymer processing, and heat energy utilization. From the above literature, no accomplishment has yet been done on the examination of ternary hybrid nanoliquid flow through an upright channel subjected to quadratic radiation, Darcy Forchheimer rule, and heat source coefficient with irreversibility analysis. The newness of the study scrutinizes the thermal energy process of ternary hybrid nanoliquid when exhibited to quadratic thermal radiation with the existence of Ti-MgO-Cu trihybrid nanoliquid. Furthermore, a comparison was made between a hybrid nanoliquid containing spherical-cylindrical nanoparticle shapes and a trihybrid nanoliquid containing spherical-cylindrical-platelet nanoparticle shapes, with the conclusion that the trihybrid nanoliquid, featuring nanoparticle shapes of spherical, cylindrical, and platelet shapes, demonstrates superior heat transfer to the hybrid nanoliquid. The study comprises the effect of corresponding parameters on entropy, velocity field, Bejan number, and thermal field have been displayed through graphs. The effect of this work is explored for the first time in the microchannel and is new and authentic.

## 2. Mathematical Formulation

Considered convective and slip flow of an incompressible, electrically, and thermally conducting ternary hybrid nanoliquid flow in a channel containing porous walled infinite parallel plates. During the flow employed external magnetic field. The uniform pressure gradient induces the flow within the channel. The occurrence of injection/suction at the right and left plates of the vertical channel separately. The left plate of the upright channel plate gets heated due to the hot fluid flow temperature  $T_w$ . The heat exchanges from the right plate to the ambient temperature  $T_b$ . The combined impact of the heat source, magnetic field, quadratic thermal radiation, and permeable media are considered to attain the energy balance equation. The representation of the above physical phenomenon is given in Fig. 1. Nanoparticles are sling separately with a base liquid such as engine oil and then found the thermal transfer and entropy production of the Ti - MgO - Cu trihybrid nanoliquid.

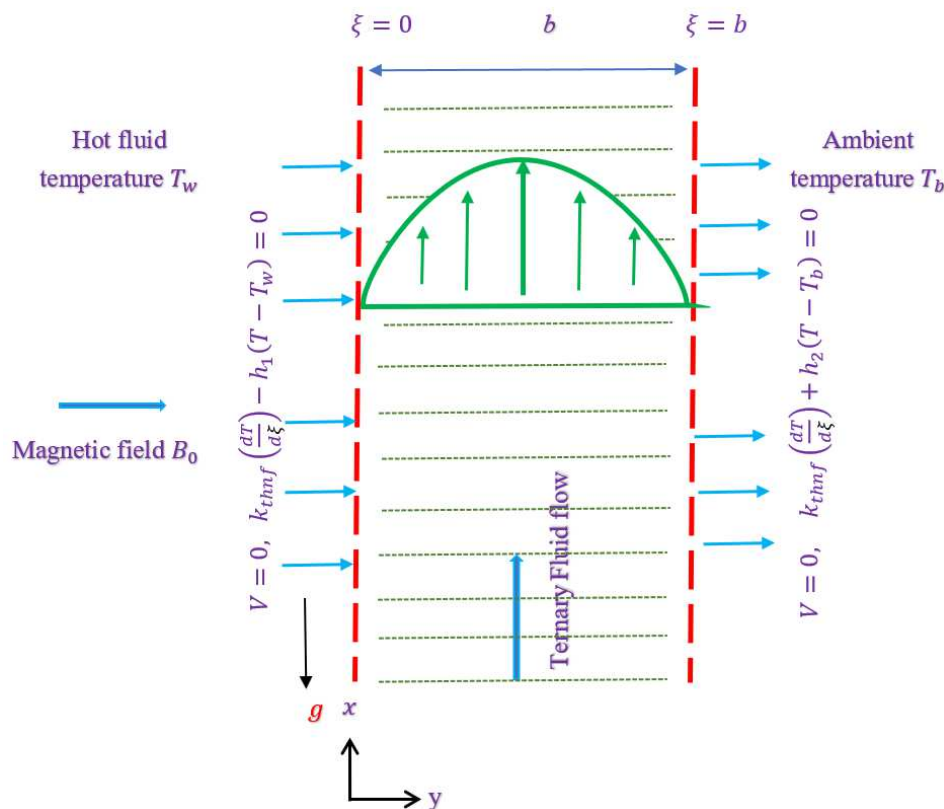


Fig. 1. Pictorial representation of flow configuration.



The momentum equation, thermal equation, and boundary conditions are as follows [19, 25, 29, 30]:

$$\rho_{thnf} \nu_0 \frac{dV}{d\xi} = -\frac{dp}{dx'} + \mu_{thnf} \frac{d^2V}{d\xi^2} - \sigma_f B_0^2 V + (\rho\beta_T)_{thnf} g^*(T - T_b) + \frac{\mu_{thnf}}{E} V - \rho_{thnf} \frac{FV^2}{\sqrt{E}}, \tag{1}$$

$$(\rho c_p)_{thnf} \nu_0 \frac{dT}{d\xi} = \left( k_{thnf} - \frac{32\sigma^* T_b^3}{3k^+} \right) \frac{d^2T}{d\xi^2} + \frac{48\sigma^* T_b^2}{3k^+} \left( \left( \frac{dT}{d\xi} \right)^2 + T \frac{d^2T}{d\xi^2} \right) + \mu_{thnf} \left( \frac{dV}{d\xi} \right)^2 + \sigma_f B_0^2 V^2 + \frac{\mu_{thnf}}{E} V^2 + \rho_{thnf} \frac{FV^3}{\sqrt{E}} + Q^+(T - T_b), \tag{2}$$

$$V = 0, \quad k_{thnf} \left( \frac{dT}{d\xi} \right) - h_1(T - T_w) = 0 \quad \text{at } \xi = 0, \tag{3}$$

$$V = 0, \quad k_{thnf} \left( \frac{dT}{d\xi} \right) + h_2(T - T_b) = 0 \quad \text{at } \xi = b. \tag{4}$$

Here,  $T$  – temperature of the liquid,  $p$  – modified pressure,  $V$  – velocity of the liquid,  $\sigma$  – electrical conductivity,  $E$  – porous medium permeability,  $\nu_0$  – suction/injection velocity,  $\rho$  – density of the fluid,  $\sigma^*$  – mean absorption coefficient,  $Q^+$  – thermal based heat source coefficient,  $k$  – thermal conductivity,  $b$  – channel width,  $T_b$  – ambient temperature,  $c_p$  is the specific heat,  $T_w$  – hot fluid temperature,  $\mu$  – viscosity of the fluid,  $h_1, h_2$  are the convective heat transfer coefficients respectively,  $F$  – Forchheimer coefficient,  $k^+$  – mean absorption coefficient, and  $B_0$  – magnetic field.

The quadratic radiation heat flux specifies by employing Rosseland approximation as follows [29, 30]:

$$q_r = -\frac{4\sigma^* dT^4}{3k^* d\xi} \cong -\frac{32\sigma^* T_b^3}{3k^*} \frac{dT}{d\xi} - \frac{24\sigma^* T_b^2}{3k^*} \frac{dT^2}{d\xi}. \tag{5}$$

The following dimensionless quantities are illuminated as:

$$W = \frac{V \rho_f b}{\mu_f}, \quad \chi = \frac{\xi}{b}, \quad \theta = \frac{T - T_b}{T_w - T_b}, \quad \theta_h = \frac{T_w}{T_b}. \tag{6}$$

By using Eq. (6) in Eqs. (1) to (4), we get:

$$\frac{\rho_{thnf}}{\rho_f} Re \frac{dW}{d\chi} = B + \frac{\mu_{thnf}}{\mu_f} \frac{d^2W}{d\chi^2} - M^2 W + \frac{(\rho\beta)_{thnf}}{(\rho\beta)_f} Gr^* \theta(\chi) - \frac{\mu_{thnf}}{\mu_f} \frac{W}{Da} - \frac{\rho_{thnf}}{\rho_f} \left( \frac{FW^2}{\sqrt{Da}} \right), \tag{7}$$

$$\frac{(\rho c_p)_{thnf}}{(\rho c_p)_f} Re Pr \frac{d\theta}{d\chi} = \left( \frac{k_{thnf}}{k_f} + Nr \right) \frac{d^2\theta}{d\chi^2} + \frac{Ec Pr}{(\theta_h - 1)} \left( \frac{\mu_{thnf}}{\mu_f} \left( \frac{dW}{d\chi} \right)^2 + \frac{\mu_{thnf}}{\mu_f} \frac{W^2}{Da} + \frac{\rho_{thnf}}{\rho_f} \left( \frac{FW^3}{\sqrt{Da}} \right) + M^2 W^2 \right) + 3Nr(\theta_h - 1) \left( \frac{d\theta}{d\chi} \right)^2 + Q\theta + 3Nr(\theta_h - 1)\theta \frac{d^2\theta}{d\chi^2} \tag{8}$$

$$W = 0, \quad \frac{k_{thnf}}{k_f} \frac{d\theta}{d\chi} - Bi(\theta - 1) = 0 \quad \text{at } \chi = 0, \tag{9}$$

$$W = 0, \quad \frac{k_{thnf}}{k_f} \frac{d\theta}{d\chi} + Bi\theta = 0 \quad \text{at } \chi = 1. \tag{10}$$

Here,  $Da = \frac{E}{b^2}$  – Darcy number,  $M^2 = \frac{\sigma_f B_0^2 b^2}{\mu_f}$  – magnetic parameter,  $Re = \frac{\rho_f \nu_0 b}{\mu_f}$  – Reynolds number,  $B = \frac{-b^3 \rho_f dp}{\mu_f^2 dx'}$  – pressure gradient parameter,  $Nr = \frac{16\sigma^* T_b^3}{3k^+ k_f}$  – radiation parameter,  $Pr = \frac{(\rho c_p)_f \mu_f}{k_f}$  – Prandtl number,  $Ec = \frac{\mu_f^2}{(\rho c_p)_f b^2 \rho_f^2 T_b}$  – Eckert number,  $Bi = \frac{bh_i}{k_f}, i = 1, 2$  – Biot number,  $Q = \frac{Q^+ b^2}{k_f}$  – thermal-dependent heat source parameter, and  $Br = Ec Pr = \frac{\mu_f^3}{k_f d^2 \rho_f^2 T_b}$  – Brinkman number.

### 2.1. Thermophysical characteristics of ternary hybrid nanoliquid

The thermophysical characteristics of ternary hybrid nanoliquid are presented in Table 1. In the current scrutiny, three variety of shaped nanoparticles such as spherical, cylindrical and platelet for the viscosity and thermal conductivity of the ternary hybrid nanoliquid is defined by the Maxwell model Arif et al. [15] and is represented below:

$$\frac{k_{nf}}{k_f} = \frac{k_p + (n - 1)k_f + (n - 1)\phi(k_p - k_f)}{k_p + (n - 1)k_f - \phi(k_p - k_f)}. \tag{11}$$

**Table 1.** Thermophysical characteristics of ternary hybrid nanoliquid [14, 15].

Viscosity	$\mu_{thnf} = \frac{\mu_f}{(1 - \phi_{s_1})^{2.5} (1 - \phi_{s_2})^{2.5} (1 - \phi_{s_3})^{2.5}}$
Density	$\frac{\rho_{thnf}}{\rho_f} = (1 - \phi_{s_1} - \phi_{s_2} - \phi_{s_3}) + \frac{\phi_{s_1} \rho_{s_1}}{\rho_f} + \frac{\phi_{s_2} \rho_{s_2}}{\rho_f} + \frac{\phi_{s_3} \rho_{s_3}}{\rho_f}$
Coefficient of thermal expansion	$\frac{(\rho\beta)_{thnf}}{(\rho\beta)_f} = (1 - \phi_{s_1} - \phi_{s_2} - \phi_{s_3}) + \frac{\phi_{s_1} (\rho\beta)_{s_1}}{(\rho\beta)_f} + \frac{\phi_{s_2} (\rho\beta)_{s_2}}{(\rho\beta)_f} + \frac{\phi_{s_3} (\rho\beta)_{s_3}}{(\rho\beta)_f}$
Heat capacity	$\frac{(\rho c_p)_{thnf}}{(\rho c_p)_f} = (1 - \phi_{s_1} - \phi_{s_2} - \phi_{s_3}) + \frac{\phi_{s_1} (\rho c_p)_{s_1}}{(\rho c_p)_f} + \frac{\phi_{s_2} (\rho c_p)_{s_2}}{(\rho c_p)_f} + \frac{\phi_{s_3} (\rho c_p)_{s_3}}{(\rho c_p)_f}$



For spherical shaped nanoparticle:

$$\frac{\mu_{nf1}}{\mu_f} = 1 + 2.5\phi + 6.2\phi^2, \quad (12a)$$

$$\frac{k_{nf1}}{k_f} = \frac{k_{s_1} + 2k_f - 2\phi(k_f - k_{s_1})}{k_{s_1} + 2k_f + \phi(k_f - k_{s_1})}. \quad (12b)$$

For cylindrical shaped nanoparticle:

$$\frac{\mu_{nf2}}{\mu_f} = 1 + 13.5\phi + 904.4\phi^2, \quad (13a)$$

$$\frac{k_{nf2}}{k_f} = \frac{k_{s_2} + 3.9k_f - 3.9\phi(k_f - k_{s_2})}{k_{s_2} + 3.9k_f + \phi(k_f - k_{s_2})}. \quad (13b)$$

For platelet shaped nanoparticle:

$$\frac{\mu_{nf3}}{\mu_f} = 1 + 37.1\phi + 612.6\phi^2, \quad (14a)$$

$$\frac{k_{nf3}}{k_f} = \frac{k_{s_3} + 4.7k_f - 4.7\phi(k_f - k_{s_3})}{k_{s_3} + 4.7k_f + \phi(k_f - k_{s_3})}. \quad (14b)$$

Since this work is concentrated on the implementations of ternary hybrid nanoliquid with distribution of three distinct nanoparticles of spherical, cylindrical, and platelet. The ternary hybrid nanoliquid is fabricated by the inclusion of the above specified nanoparticles in the engine oil. For the effectuality of the current model nanoliquid expression has been attained by taking into consideration the technique of interpolation which is shape factor and concentration dependent on the nanoparticles 1, 2, and 3 which is denoted by  $\phi_{s_1}$ ,  $\phi_{s_2}$  and  $\phi_{s_3}$  and the total combined volume of the nanoparticles in bulk is denoted as  $\phi = \phi_{s_1} + \phi_{s_2} + \phi_{s_3}$ .

The expression for the viscosity and thermal conductivity of the ternary hybrid nanoliquid drafted below:

$$\mu_{thnf} = \frac{\phi_{s_1}\mu_{nf1} + \phi_{s_2}\mu_{nf2} + \phi_{s_3}\mu_{nf3}}{\phi} \quad \text{and} \quad k_{thnf} = \frac{\phi_{s_1}k_{nf1} + \phi_{s_2}k_{nf2} + \phi_{s_3}k_{nf3}}{\phi}.$$

### 3. Irreversibility Analysis

The local entropy production is defined by [19, 25, 29, 30]:

$$Eg^* = \frac{1}{T^2} \left( \frac{dT}{d\xi} \right)^2 \left( k_{thnf} + \frac{48\sigma^* T_b^2 T}{3k^+} - \frac{32\sigma^* T_b^3}{3k^+} \right) + \frac{\mu_{thnf}}{T} \left( \frac{dV}{d\xi} \right)^2 + \frac{\sigma_f B_0^2 V^2}{T} + \frac{\mu_{thnf} V^2}{T E} + \frac{\rho_{thnf} F V^3}{T \sqrt{E}}. \quad (15)$$

The above-mentioned equation takes the non-dimensional form as follows:

$$Eg = \frac{(\theta_h - 1)^2}{[\theta(\theta_h - 1) + 1]^2} \left( \frac{k_{thnf}}{k_f} + Nr[3\theta(\theta_h - 1) + 1] \right) \left( \frac{d\theta}{d\chi} \right)^2 + \frac{EcPr}{[\theta(\theta_h - 1) + 1]} \left( \frac{\mu_{thnf}}{\mu_f} \left( \frac{dW}{d\chi} \right)^2 + M^2 W^2 + \frac{\mu_{thnf} W^2}{\mu_f Da} + \frac{\rho_{thnf} F W^3}{\rho_f \sqrt{Da}} \right). \quad (16)$$

where  $Eg^*$  and  $Eg$  are the dimensional and non-dimensional irreversibility and  $Eg^*$  is normalized by  $\frac{v_f^2}{k_f}$ .

On the right-hand side, the irreversibility due to thermal transfer process, fluid friction, Ohmic heating, Darcy and Forchheimer friction drag are represented 1<sup>st</sup>, 2<sup>nd</sup>, 3<sup>rd</sup>, 4<sup>th</sup> and 5<sup>th</sup> terms, respectively.

Here,

$$N_1 = \frac{(\theta_h - 1)^2}{[\theta(\theta_h - 1) + 1]^2} \left( \frac{k_{thnf}}{k_f} + Nr[3\theta(\theta_h - 1) + 1] \right) \left( \frac{d\theta}{d\chi} \right)^2 \quad \text{is heat transfer irreversibility,} \quad (17a)$$

$$N_2 = \frac{EcPr}{[\theta(\theta_h - 1) + 1]} \left( \frac{\mu_{thnf}}{\mu_f} \left( \frac{dW}{d\chi} \right)^2 + M^2 W^2 + \frac{\mu_{thnf} W^2}{\mu_f Da} + \frac{\rho_{thnf} F W^3}{\rho_f \sqrt{Da}} \right) \quad \text{is dissipative irreversibility.} \quad (17b)$$

Bejan number is defined as:

$$Be = \frac{\text{Heat transfer irreversibility}}{\text{Total irreversibility}}, \quad (18a)$$

$$Be = \frac{(\theta_h - 1)^2}{[\theta(\theta_h - 1) + 1]^2} \left( \frac{k_{thnf}}{k_f} + Nr[3\theta(\theta_h - 1) + 1] \right) \left( \frac{d\theta}{d\chi} \right)^2}{Eg}. \quad (18b)$$





### 4. Numerical Procedure

Equations (7) and (8) featuring boundary conditions outlined in Eqs. (9) and (10) have been modified to a set of nonlinear first order ordinary differential equations that have certain unspecified initial conditions that are determined using the shooting process. The aforementioned equations are resolved with the Runge Kutta Fehlberg approach.

To ensure accuracy in the solution of an initial value problem, solve it twice with step sizes  $h$  and  $\frac{h}{2}$ . However, for lower step sizes, this approach necessitates a significant amount of simulation and must be repeated until the results are satisfactory. The current numerical system, the Runge-Kutta Fehlberg scheme, is one such approach that includes a process for determining if the appropriate step size is employed. At each stage, two different approximations of a solution are obtained and compared. If the two solutions line up close enough, the derived approximation is accepted; otherwise, the step size is lowered. If the solution corresponds with more significant digits, then the step size will be increased.

Listed below six values are achieved at each step:

$$\begin{aligned}
 m_1 &= h f(x_1, y_1), \\
 m_2 &= h f\left(x_1 + \frac{1}{4}h, y_1 + \frac{1}{4}m_1\right), \\
 m_3 &= h f\left(x_1 + \frac{3}{8}h, y_1 + \frac{3}{32}m_1 + \frac{9}{32}m_2\right), \\
 m_4 &= h f\left(x_1 + \frac{12}{13}h, y_1 + \frac{1932}{2197}m_1 - \frac{7200}{2197}m_2 + \frac{7296}{2197}m_3\right), \\
 m_5 &= h f\left(x_1 + h, y_1 + \frac{439}{216}m_1 - 8m_2 + \frac{3680}{513}m_3 - \frac{845}{4104}m_4\right), \\
 m_6 &= h f\left(x_1 + \frac{1}{2}h, y_1 - \frac{8}{27}m_1 + 2m_2 - \frac{3544}{2565}m_3 - \frac{1859}{4104}m_4 - \frac{11}{40}m_5\right).
 \end{aligned}
 \tag{19}$$

Then, an estimation employing the fourth order Runge-Kutta technique is:

$$y_{m+1} = y_1 + \frac{25}{216}m_1 + \frac{1408}{2565}m_3 + \frac{2197}{4101}m_4 - \frac{1}{5}m_5.
 \tag{20}$$

Another value of  $y$  is obtained implementing the fifth order Runge-Kutta technique outlined below:

$$z_{m+1} = y_1 + \frac{16}{135}m_1 + \frac{6656}{12825}m_3 + \frac{28561}{56430}m_4 - \frac{9}{50}m_5 + \frac{2}{55}m_6.
 \tag{21}$$

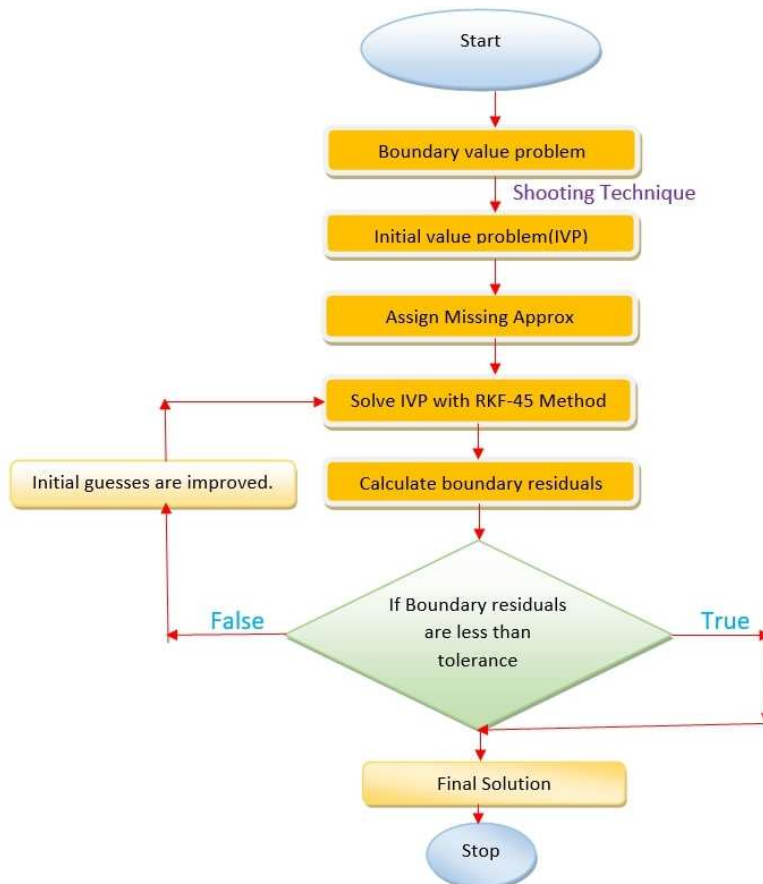


Fig. 2. Flow chart of the present problem.



**Table 2.** Nanoparticles and base fluids thermophysical characteristics [22].

	$\rho(\text{kgm}^{-3})$	$C_p(\text{Jkg}^{-1}\text{K}^{-1})$	$k(\text{Wm}^{-1}\text{K}^{-1})$	$\beta(\text{K}^{-1}) \times 10^{-5}$	Shape
$Ti (s_1)$	4510	540	20.9	0.9	Spherical
$MgO (s_2)$	3560	955	45	1.26	Cylindrical
$Cu (s_3)$	8933	385	400	5.1	Platelet
Engine oil (EO) (f)	884	1910	0.144	70	-

**Table 3.** Comparison of flow field when  $Gr = Nr = 0, Re = B = 1$  [20].

$\chi$	$W(\chi)$ FEM	$W(\chi)$ RKF (present)
0	0.0	0.0
0.2	0.07114875	0.07114876
0.4	0.11376948	0.11376948
0.6	0.12154600	0.12154601
0.8	0.08676372	0.08676373
1.0	0.0	0.0

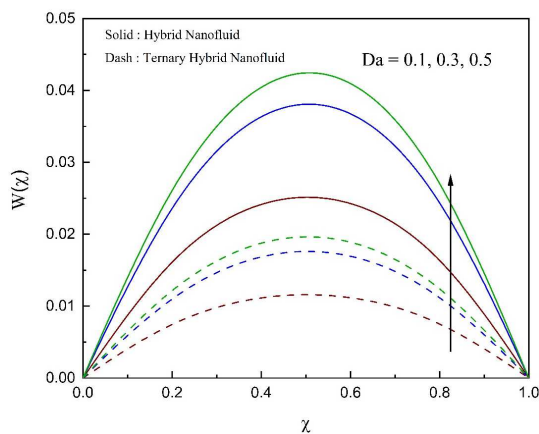
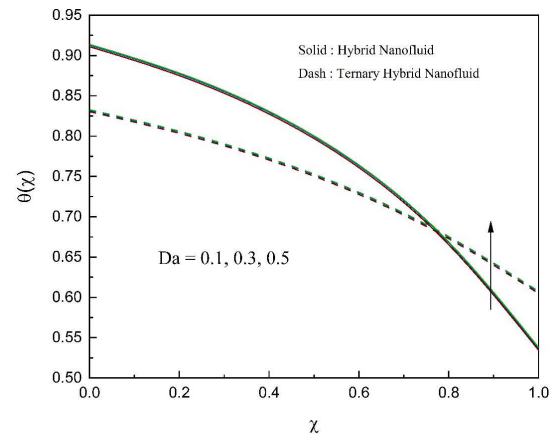
If  $|y_{m+1} + z_{m+1}|$  is small enough, then the procedure is ceased. Otherwise, the simulation will continue with a smaller step size  $h$ . This approach has a local truncation error of  $|y_{m+1} - z_{m+1}|$ .

If the attained value is small enough, then the simulation is terminated or else carried out by utilizing a smaller step size and meets the convergence condition  $10^{-6}$  by reducing step size. Figure 2 elucidates the pictorial representation of flow chart.

## 5. Results and Discussion

The existing investigation aims to conceptualize the physical analysis of liquid flow parameters and their influence on ternary hybrid nanoliquid. In this exploration distinct nanoparticles with shape effect in a base liquid engine oil have been considered, in particular ternary hybrid nanoliquid. Comparative scrutiny of hybrid nanoliquid  $Ti - MgO/EO$  and trihybrid nanoliquid  $Ti - MgO - Cu/EO$  is carried out for various concerning parameters. In the base liquid engine oil concoction of spherical shaped titanium ( $Ti$ ), cylindrical shaped magnesium oxide ( $MgO$ ) and platelet shaped copper ( $Cu$ ) nanoparticles are considered. By using the Runge-Kutta Fehlberg 4th-5th order technique by way of the shooting approach, the transformed nondimensional momentum, and thermal mathematical models (7) and (8) with suitable boundary conditions (9) and (10) are computed. The consequences of involved physical parameters such as radiation parameter ( $Nr$ ), temperature parameter ( $\theta_h$ ), heat source parameter ( $Q$ ), Biot number ( $Bi$ ), magnetic parameter ( $M$ ), Eckert number ( $Ec$ ), volume fraction nanoparticles ( $\phi$ ), Reynolds number ( $Re$ ), Prandtl number ( $Pr$ ), Darcy number ( $Da$ ), and Forchheimer coefficient ( $F$ ) are explored in the field of temperature  $\theta(\chi)$ , velocity  $W(\chi)$ , Bejan number  $Be(\chi)$ , and entropy generation  $Eg(\chi)$ . Throughout this analysis for the numerical computations, the magnitude of the parameters is set as:  $Bi = 2, B = 1, Ec = 0.5, F = 5, Q = 0.1, Pr = 6.2, Re = 1, Gr = 0.5, M = 0.5, Da = 0.1, \phi_{s_1} = \phi_{s_2} = \phi_{s_3} = 0.03, \theta_h = 2, Nr = 1$ . Base liquid and nanoparticle thermophysical characteristics are illustrated in Table 2. Comparison between FEM and RKF method for the velocity field are depicted in Table 3 (Madhu et al. [20]).

All the graphical representations show the flow chart of the ternary hybrid nanoliquid and hybrid nanoliquid the mixture of nanoparticles in the engine oil base liquid. Figures 3 to 6 manifest the influence of Darcy number on the velocity field  $W(\chi)$ , thermal field  $\theta(\chi)$ , entropy  $Eg(\chi)$ , and Bejana number  $Be(\chi)$ . It is noted from Fig. 3 that the velocity field escalates with a greater magnitude of Darcy number. The reason behind this is the inclusion of pores into the channel makes fluid flow quite easier. The consequences of Darcy number on the thermal field in Fig. 4. The growth in temperature profile absorbed towards heightened Darcy number. This is due to the viscous heating of the fluid flow. Figures 5 and 6 elaborate on the significant influence of Darcy number on entropy and Bejan number. As the Darcy number intensifies, the entropy production is exaggerated with the Darcy number, but the Bejan number shows decreasing behavior for the same Darcy number. This is due to the fact that the improved value of the Darcy number boosts the permeability parameter of the porous media, as a result, the nanoliquid flows with higher velocity.

**Fig. 3.** Impression of Darcy number on flow profile.**Fig. 4.** Impression of Darcy number on thermal profile.

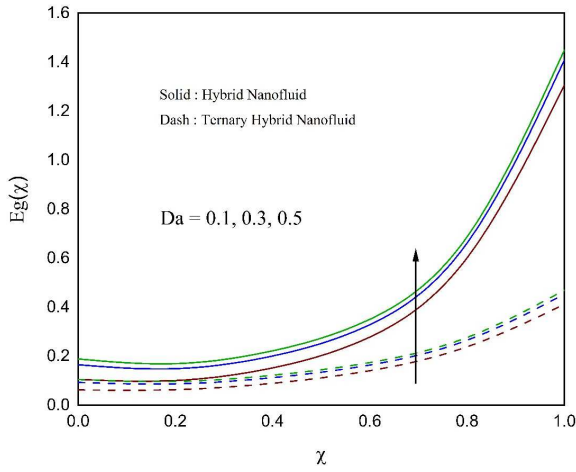


Fig. 5. Impression of Darcy number on entropy profile.

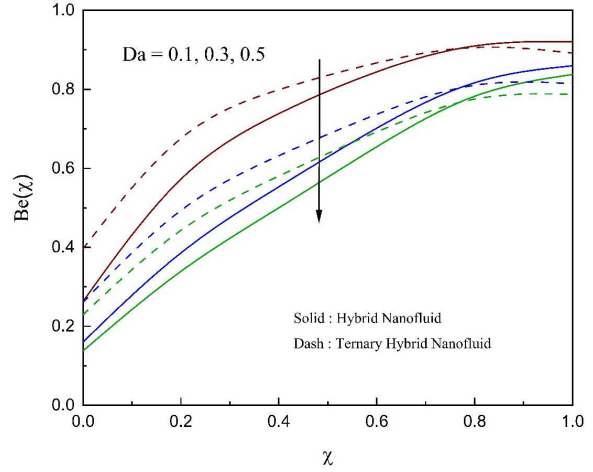


Fig. 6. Impression of Darcy number on Bejan number.

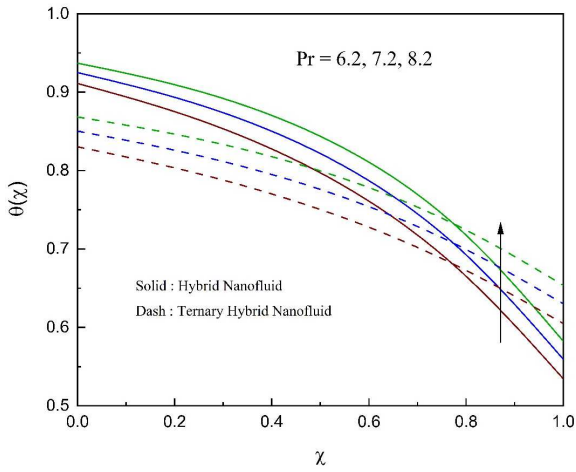


Fig. 7. Impression of Prandtl number on thermal profile.

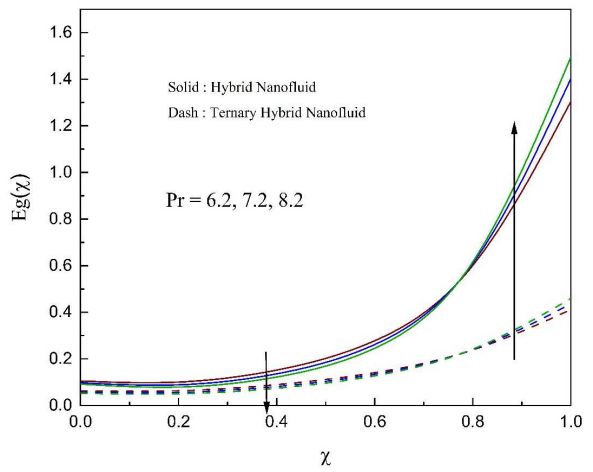


Fig. 8. Impression of Prandtl number on entropy profile.

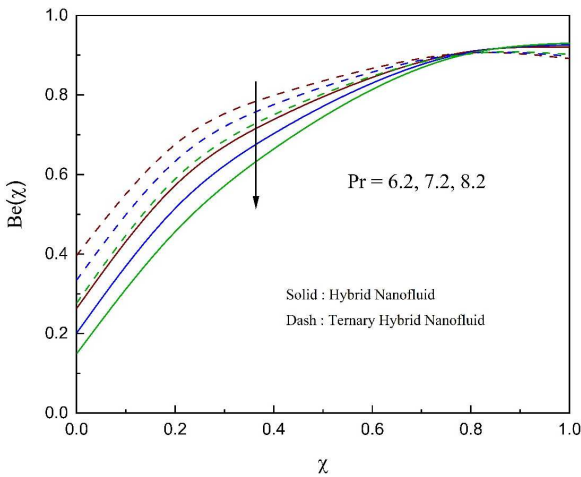


Fig. 9. Impression of Prandtl number on Bejan number.

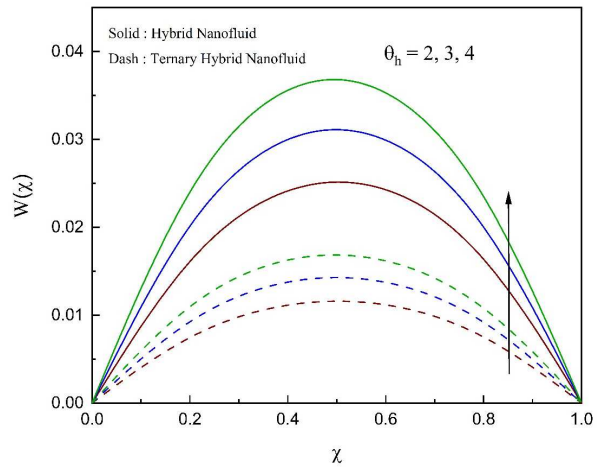


Fig. 10. Impression of temperature parameter on flow profile.

The consequences of thermal profile  $\theta(\chi)$ , entropy  $Eg(\chi)$ , and Bejan number  $Be(\chi)$  of engine oil based ternary hybrid nanofluid profiles for distinct values of Prandtl number are exhibited in Figs. 7 to 9. Figure 7 depicts the effect of the Prandtl number on the temperature profile. It is observed from the graph that the escalated Prandtl number boosts the thermal field. Increasing the Prandtl number, which represents the ratio of viscous diffusion to thermal rate, leads to an increase in temperature profile due to increased heat transfer to the surroundings. Figure 8 shows the impression of the Prandtl number on entropy. It is very clear from the graph, that the entropy production declines at the left and up to mid of the channel but enhances at the end of the channel for the improved Prandtl number. Figure 9 demonstrates the consequences of the Prandtl number on the Bejan number. It is noticeably concluded that the Bejan number significantly declines at the left wall of the channel, but the opposite nature is seen at the other part of the channel on the intensified magnitude of the Prandtl number.





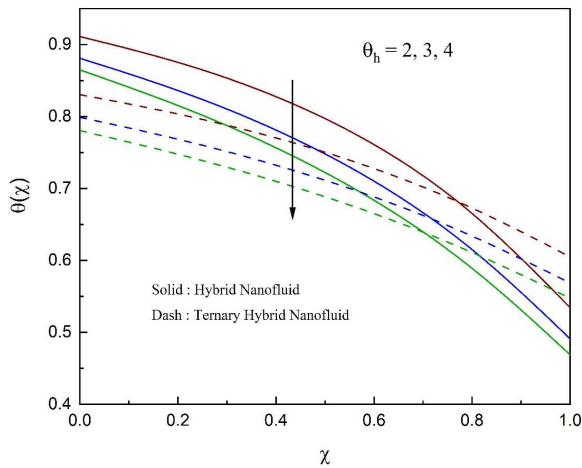


Fig. 11. Impression of temperature parameter on thermal profile.

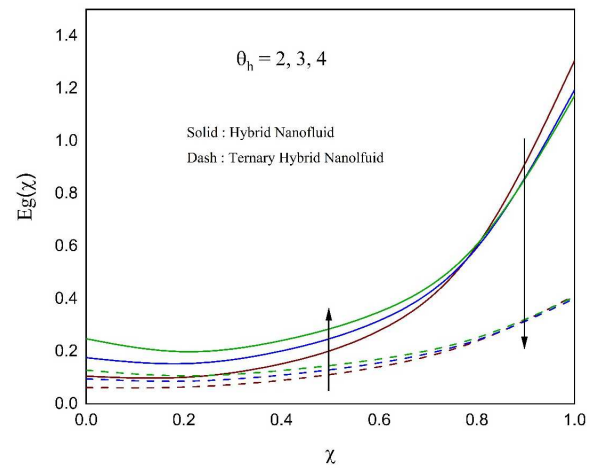


Fig. 12. Impression of temperature parameter on entropy profile.

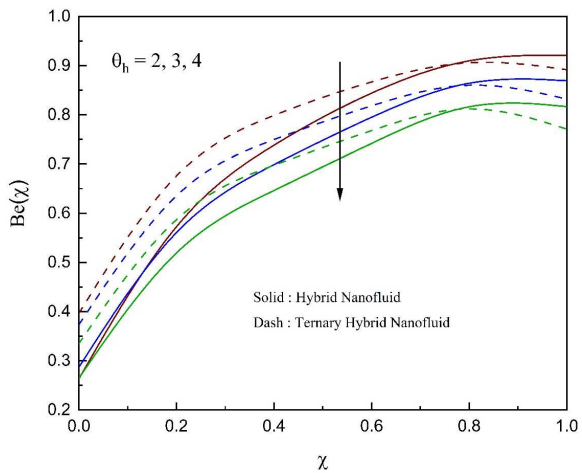


Fig. 13. Impression of temperature parameter on Bejan number.

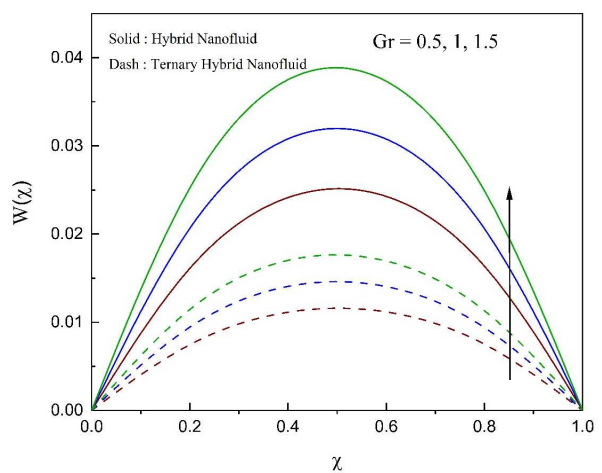


Fig. 14. Impression of Grashof number on flow profile.

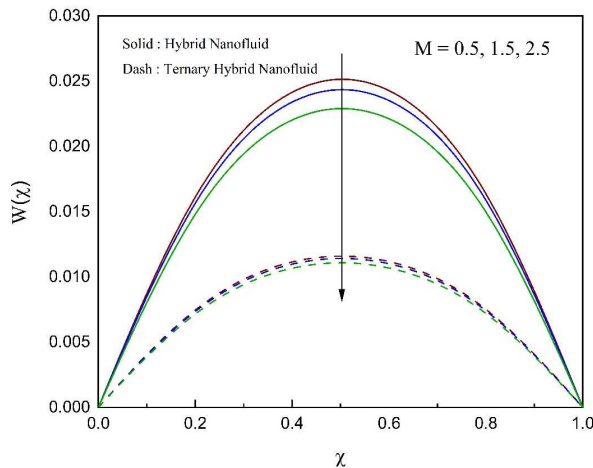


Fig. 15. Impression of magnetic parameter on flow profile.

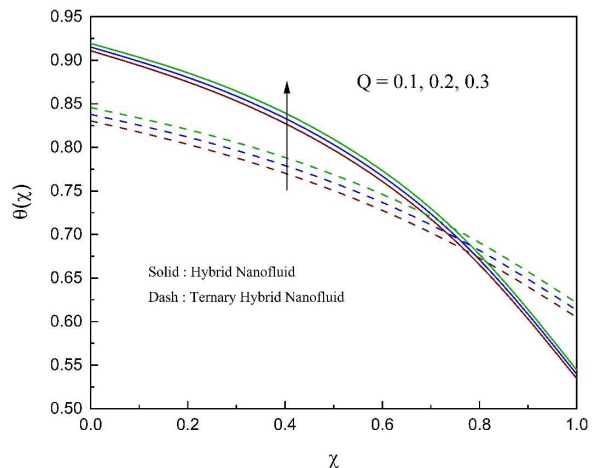


Fig. 16. Impression of heat source parameter on thermal profile.

The influence of flow field  $W(\chi)$ , thermal profile  $\theta(\chi)$ , entropy  $Eg(\chi)$ , and Bejan number  $Be(\chi)$  of engine oil based ternary hybrid nanoliquid and hybrid nanoliquid profiles for distinct values of temperature parameter is exhibited in Figs. 10 to 13. The impact of temperature parameter on the velocity field is shown in Fig. 10. The velocity field is enhanced with improved temperature parameter. The noticeable decrement of thermal field is noted towards enhanced temperature parameter in Fig. 11. Figures 12 and 13 exemplify the behavior of entropy and Bejan number on the heightened magnitude of temperature parameter. The thermal transfer process generates more molecular randomness as the temperature parameter increases. Entropy production is increased at the channel's left wall while decreasing at another portion of the channel with an improved temperature parameter. The permeable plate enriches the temperature of the injected fluid, which accounts for this. The temperature parameter inflates the thermal transfer rate. Hence more molecular randomness occurs. Also noted is that the Bejan number diminishes with improved temperature parameter.



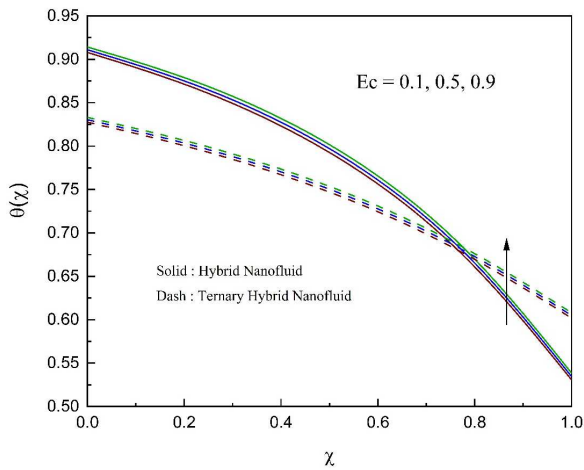


Fig. 17. Impression of Eckert number on thermal profile.

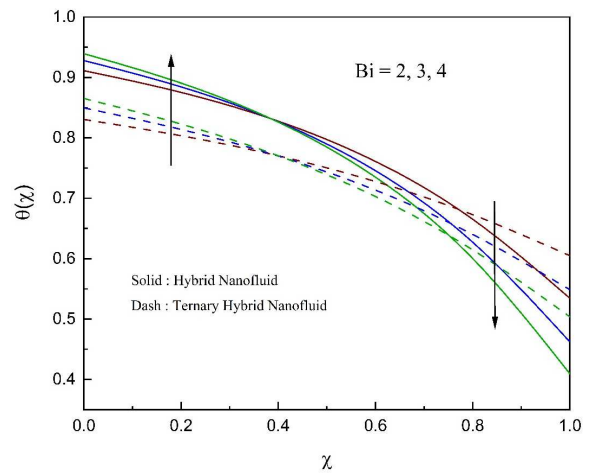


Fig. 18. Impression of Biot number on thermal profile.

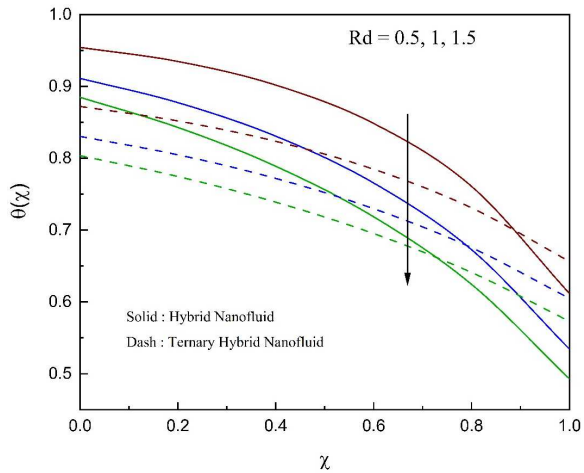


Fig. 19. Impression of radiation parameter on thermal profile.

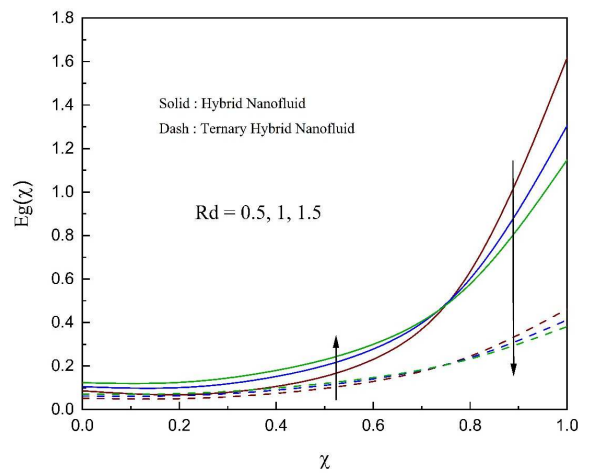


Fig. 20. Impression of radiation parameter on entropy profile.

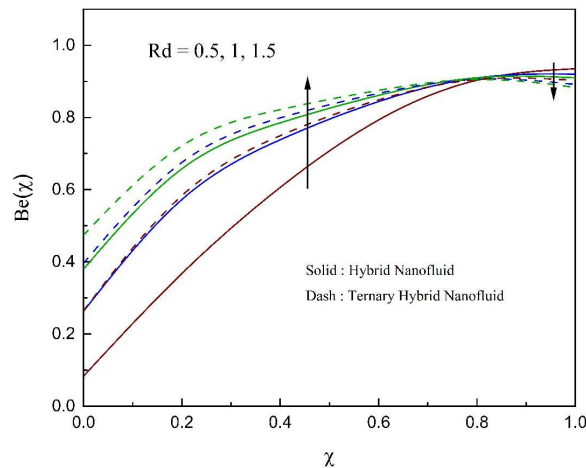


Fig. 21. Impression of radiation parameter on Bejan number.

Figure 14 depicts the impact of the Grashof number on the velocity field  $W(\chi)$ . It is noticed that the increased Grashof number significantly affects the velocity field. The physical reason for this velocity profile behavior can be explained by the Grashof number, which represents the ratio of buoyancy forces to inertial forces. When the Grashof number is higher, buoyancy forces exert a stronger influence, resulting in more pronounced convectational effects. In other words, increased buoyancy forces have a larger impact on the fluid's overall velocity profiles. Figure 15 explains the velocity field  $W(\chi)$  against the Hartmann number. The Hartmann number resulted in a decrement in the velocity profile. This is because the fluid flow is resisted by Lorentz force by opposing the liquid motion in a channel. Figure 16 depicts the amplified character of the temperature observed towards the inflated heat source parameter due to a boost in internal heat. This is because as the heat source parameter intensifies internal heat of the nanofluid increases. Figure 17 shows the temperature of the liquid augmented as the Eckert number elevates. It is noted from the graph, that the Eckert number has a disposition to lessen the temperature in the channel. It is possible to surmise that the fluid



thermal conductivity downturned by magnifying the momentum diffusivity ratio to thermal diffusivity. Therefore, the thermal transfer declines with the channel. From Fig. 18, it is sensibly noticed that the temperature profile increases at the left wall and dramatically declines at the other part of the channel for the higher value of the Biot number. This is due to the fact that the thermal transport takes place from the hot nanoparticles to comparable cold nanoparticles. Efficacious cooling is cherished by convection.

Figures 19 to 21 demonstrates the influence of radiation parameter on thermal field  $\theta(\chi)$ , entropy  $Eg(\chi)$ , and Bejan number  $Be(\chi)$ . Reduced magnitude of temperature is observed for the improved radiation parameter. This is because of the greater value of heat flux from the left to the right upright plate which is in touch with atmospheric circumambient temperature which is shown in Fig. 19. The dual behaviour of entropy on enhanced radiation parameter is noted in Fig. 20. Because of the higher influence of fluid friction irreversibility. The entropy production inflates from the left to the middle of the channel and depletes at the right part of the channel with an enhanced magnitude of radiation parameter. Figure 21 illustrates the Bejan number upsurges at left and up to mid of the channel and shows decremental order at another part of the channel due to the noticeable influence of viscous dissipation.

## 6. Conclusion

In this current study, the thermal and entropy analysis in a shape dependent ternary hybrid nanoliquid flow in an upright microchannel was investigated along with quadratic thermal radiation, Darcy-Forchheimer rule, heat source coefficient, buoyancy force and no slip condition. The considerable outcomes of the present exploration are as follows:

- Improved Grashof number leads to an intensified velocity field, but the opposite effect is observed with magnetic constraints.
- Ternary hybrid nanoliquid exhibits a stronger thermal field with a higher Eckert number and heat source parameter.
- Augmentation of quadratic radiation parameter leads to an intensification of entropy production in the left and declines in another wall of the channel, also same behaviour seen for the Bejan number.
- Entropy production shows increasing behaviour towards enhanced temperature parameter.
- Along the length of the microchannel, the thermal field is affected by the shape of nanoparticles. Particularly, in the case of trihybrid nanoliquid consisting of spherical, cylindrical and platelet shaped nanoparticles, the highest temperature distribution was noticed. And surpassing thermal distribution attained by the mixture of spherical and cylindrical shaped nanoparticles in the hybrid nanoliquid.
- With an enhanced darcy number of 400%, the Entropy generation rises by 14% in the ternary hybrid nanoliquid circumstances and rises by 11% in the hybrid nanoliquid situation.
- The comparative study between hybrid and ternary hybrid nanoliquid discloses that an uplifted thermal transfer rate and Bejan number are noticed in trihybrid nanoliquid.

This present study can be extended to different shapes of nanoparticles and effect of Buongiorno model. The work limitations are as follows: we have assumed the flow is steady, laminar and the fluid is viscous and incompressible.

## Author Contributions

B.J. Gireesha: Formal Analysis, Methodology. L. Anitha: Writing of the original draft, Conceptualization, Methodology. The authors read and approved the final version of the manuscript.

## Acknowledgments

Not applicable.

## Conflict of Interest

The authors declared no potential conflicts of interest with respect to the research, authorship, and publication of this article.

## Funding

The authors received no financial support for the research, authorship, and publication of this article.

## Data Availability Statements

The datasets generated and/or analyzed during the current study are available from the corresponding author on reasonable request.

## Nomenclature

$Q^+$	Heat source coefficient	$T_b$	Ambient temperature ( $K$ )
$Ec$	Eckert number	$b$	Channel width ( $m$ )
$V(\xi)$	Dimensional fluid velocity ( $m/s$ )	$Re$	Reynolds number
$Be$	Bejan number	$Q'$	Heat source parameter
$h_1, h_2$	Coefficient of convective heat transfer ( $W/m^2K$ )	$W(\chi)$	Dimensionless fluid velocity



$Nr$	Radiation parameter	$Eg(\chi)$	Dimensionless entropy generation
$q_r$	Radiative heat flux ( $W/m^2$ )	$M$	Magnetic parameter
$k^+$	Mean absorption coefficient ( $m^{-1}$ )	$B_0$	Magnetic field strength ( $Am^{-1}$ )
$T$	Fluid temperature ( $K$ )	$T_w$	Hot fluid temperature ( $K$ )
$N_2$	Dissipative irreversibility	$p$	Pressure ( $kgm^{-1}s^{-2}$ )
$Eg^*$	Entropy generation ( $JK^{-1}$ )	$c_p$	Specific heat ( $Jkg^{-1}K^{-1}$ )
$Pr$	Prandtl number	$B$	Pressure gradient parameter
$k$	Thermal conductivity ( $W/mK$ )	$N_1$	Heat transfer irreversibility
$Da$	Darcy number	$F$	Forchheimer coefficient
$Br$	Brinkman number	$Bi$	Biot number
<b>Greek symbols</b>			
$\xi$	Transverse coordinate ( $m$ )	$\phi$	Solid volume fraction of nanoparticles
$\sigma^*$	Stefan-Boltzmann constant ( $Wm^{-2}K^{-4}$ )	$\nu$	Kinematic viscosity of the fluid ( $m^2s^{-1}$ )
$\rho$	Density of the fluid ( $kgm^{-3}$ )	$\nu_0$	Velocity suction/injection ( $m/s$ )
$\sigma$	Electrical conductivity ( $A^2s^3m^{-3}kg^{-1}$ )	$\chi$	Dimensionless transverse coordinate
$\theta$	Dimensionless temperature	$\mu$	Dynamic viscosity ( $kgm^{-1}s^{-1}$ )
<b>Subscripts</b>			
1, 2	Left plate and right plate respectively	$s_3$	Cu nanoparticles
$f$	Fluid	$s_1$	Ti nanoparticles
$tnf$	Ternary hybrid nanofluid	$s_2$	MgO nanoparticles


## References

- [1] Yang, C., Ng, C.B., Chan, V., Transient Analysis of Electroosmotic Flow in a Slit Microchannel, *Journal of Colloid and Interface Science*, 248(2), 2002, 524-527.
- [2] Meisel, I., Ehrhard, P., Electrically-excited (electroosmotic) flows in microchannels for mixing applications, *European Journal of Mechanics B/Fluids*, 25, 2006, 491-504.
- [3] Sbragaglia, M., Prosperetti, A., A note on the effective slip properties for microchannel flows with ultra-hydrophobic surfaces, *Physics of Fluids*, 19(4), 2007, 043603.
- [4] Cho, E.S., Choi, J.W., Yoon, J.S., Kim, M.S., Modeling and simulation on the mass flow distribution in microchannel heat sinks with non-uniform heat flux conditions, *International Journal of Heat and Mass Transfer*, 53(7-8), 2010, 1341-1348.
- [5] Kalteh, M., Investigating the effect of various nanoparticle and base liquid types on the nanofluids heat and fluid flow in a microchannel, *Applied Mathematical Modelling*, 37(18-19), 2013, 8600-8609.
- [6] Ibanez, G., Lopez, A., Pantoja, J., Moreira, J., Entropy generation analysis of a nanofluid flow in MHD porous microchannel with hydrodynamic slip and thermal radiation, *International Journal of Heat and Mass Transfer*, 100, 2016, 89-97.
- [7] Sharaf, O.Z., Al-Khateeb, A.N., Kyritsis, D.C., Abu-Nada, E., Numerical investigation of nanofluid particle migration and convective heat transfer in microchannels using an Eulerian-Lagrangian approach, *Journal of Fluid Mechanics*, 878(10), 2019, 62-97.
- [8] Moshfegh, A., Abouei Mehri, A., Javadzadegan, A., Joshaghani, M., Ghasemi-Fare, O., Numerical investigation of various nanofluid heat transfers in microchannel under the effect of partial magnetic field: lattice Boltzmann approach, *Journal of Thermal Analysis and Calorimetry*, 140, 2020, 773-787.
- [9] Sindhu, S., Gireesha, B.J., Entropy generation analysis of hybrid nanofluid in a microchannel with slip flow, convective boundary and nonlinear heat flux, *International Journal of Numerical Methods for Heat & Fluid Flow*, 31(1), 2021, 53-74.
- [10] Abbasi, A., Al-Khaled, K., Khan, M.I., Khan, S.U., El-Refaey, A.M., Farooq, W., Jameel, M., Qayyum, S., Optimized analysis and enhanced thermal efficiency of modified hybrid nanofluid (Al<sub>2</sub>O<sub>3</sub>, CuO, Cu) with nonlinear thermal radiation and shape features, *Case Studies in Thermal Engineering*, 28, 2021, 101425.
- [11] Smrity, A.M.A., Yin, P., Design and performance evaluation of pulsating heat pipe using metallic nanoparticles based hybrid nanofluids, *International Journal of Heat and Mass Transfer*, 218, 2024, 124773.
- [12] Dezfulizadeh, A., Aghaei, A., Joshaghani, A.H., Najafizadeh, M.N., An experimental study on dynamic viscosity and thermal conductivity of water-Cu-SiO<sub>2</sub>-MWCNT ternary hybrid nanofluid and the development of practical correlations, *Powder Technology*, 389, 2021, 215-234.
- [13] Boroomandpour, A., Toghraie, D., Hashemian, M., A comprehensive experimental investigation of thermal conductivity of a ternary hybrid nanofluid containing MWCNTs- titania-zinc oxide/water ethylene glycol (80:20) as well as binary and mono nanofluids, *Synthetic Metals*, 268, 2020, 116501.
- [14] Das, S., Ali, A., Jana, R.N., Makinde, O.D., EDL impact on mixed magneto-convection in a vertical channel using ternary hybrid nanofluid, *Chemical Engineering Journal Advances*, 12, 2022, 100412.
- [15] Arif, M., Di Persio, L., Kumam, P., Watthayu, W., Akgül, A., Heat transfer analysis of fractional model of couple stress Casson tri-hybrid nanofluid using dissimilar shape nanoparticles in blood with biomedical applications, *Scientific Reports*, 13, 2023, 4596.
- [16] Mohanty, D., Mahanta, G., Shaw, S., Irreversibility and thermal performance of nonlinear radiative cross-ternary hybrid nanofluid flow about a stretching cylinder with industrial applications, *Powder Technology*, 433, 2024, 119255.
- [17] Hamdan, M.A., Al-Assaf, A.H., Al-Nimr, M.A., The Effect of Slip Velocity and Temperature Jump on the Hydrodynamic and Thermal Behaviors of MHD Forced Convection Flows in Horizontal Microchannels, *Iranian Journal of Science and Technology, Transactions of Mechanical Engineering*, 40, 2016, 95-103.
- [18] Mozaffari, M., D'Orazio, A., Karimpour, A., Abdollahi, A., Safae, M.R., Lattice Boltzmann method to simulate convection heat transfer in a microchannel under heat flux Gravity and inclination angle on slip-velocity, *International Journal of Numerical Methods for Heat & Fluid Flow*, 30(6), 2020, 3371-3398.
- [19] Venkateswarlu, M., Bhaskar, P., Entropy Generation and Bejan Number Analysis of MHD Casson Fluid Flow in a Micro-Channel with Navier Slip and Convective Boundary Conditions, *International Journal of Thermofluid Science and Technology*, 7(4), 2020, 070403.
- [20] Madhu, M., Mahanthesh, B., Shashikumar, N.S., Shehzad, S.A., Khan, S.U., Gireesha, B.J., Performance of second law in Carreau fluid flow by an inclined microchannel with radiative heated convective condition, *International Communications in Heat and Mass Transfer*, 117, 2020, 104761.
- [21] Ebrahimi, A., Rikhtegar, F., Sabaghan, A., Roohi, E., Heat transfer and entropy generation in a microchannel with longitudinal vortex generators using nanofluids, *Energy*, 101, 2016, 190-201.



- [22] Ranjit, N.K., Shit, G.C., Tripathi, D., Entropy generation and Joule heating of two layered electroosmotic flow in the peristaltically induced microchannel, *International Journal of Mechanical Sciences*, 153–154, 2019, 430–444.
- [23] Siva, T., Jangili, S., Kumbhakar, B., Siva, T., Jangili, S., Kumbhakar, B., Analytical solution to optimise the entropy generation in EMHD flow of non-Newtonian fluid through a microchannel, *Pramana – Journal of Physics*, 96, 2022, 168.
- [24] Anitha, L., Gireesha, B.J., Convective flow of Jeffrey nanofluid along an upright microchannel with Hall current and Buongiorno model: an irreversibility analysis, *Applied Mathematics and Mechanics (English Edition)*, 44, 2023, 1613–1628.
- [25] Hayat, T., Haider, F., Muhammad, T., Hayat, T., Haider, F., Muhammad, T., Darcy–Forchheimer flow of carbon nanotubes due to a convectively heated rotating disk with homogeneous–heterogeneous reactions, *Journal of Thermal Analysis Calorimetry*, 137, 2019, 1939–1949.
- [26] Misra, J.C., Mallick, B., Steinmann, P., Temperature distribution and entropy generation during Darcy–Forchheimer–Brinkman electrokinetic flow in a microfluidic tube subject to a prescribed heat flux, *Meccanica*, 55, 2020, 1079–1098.
- [27] Jakeer, S., Basha, H.T., Reddy, S.R.R., Abbas, M., Alqahtani, M.S., Loganathan, K., Vivek Anand, A., Entropy analysis on EMHD 3D micropolar trihybrid nanofluid flow of solar radiative slendering sheet by a machine learning algorithm, *Scientific Reports*, 13, 2023, 19168.
- [28] Shaw, S., Samantaray, S.S., Misra, A., Nayak, M.K., Makinde, O.D., Hydromagnetic flow and thermal interpretations of Cross hybrid nanofluid influenced by linear, nonlinear and quadratic thermal radiations for any Prandtl number, *International Communications in Heat and Mass Transfer*, 130, 2022, 105816.
- [29] Rana, P., Gupta, S., Gupta, G., Unsteady nonlinear thermal convection flow of MWCNT–MgO/EG hybrid nanofluid in the stagnation-point region of a rotating sphere with quadratic thermal radiation: RSM for optimization, *International Communications in Heat and Mass Transfer*, 134, 2022, 106025.
- [30] Gupta, G., Rana, P., Comparative Study on Rosseland’s Heat Flux on Three-Dimensional MHD Stagnation-Point Multiple Slip Flow of Ternary Hybrid Nanofluid over a Stretchable Rotating Disk, *Mathematics*, 10(18), 2022, 3342.
- [31] Chen, H., He, P., Shen, M., Ma, Y., Thermal analysis and entropy generation of Darcy–Forchheimer ternary nanofluid flow: A comparative study, *Case Studies in Thermal Engineering*, 43, 2023, 102795.

## ORCID iD

B.J. Gireesha  <https://orcid.org/0000-0002-4761-1082>

L. Anitha  <https://orcid.org/0009-0008-7204-6549>



© 2024 Shahid Chamran University of Ahvaz, Ahvaz, Iran. This article is an open access article distributed under the terms and conditions of the Creative Commons Attribution-NonCommercial 4.0 International (CC BY-NC 4.0 license) (<http://creativecommons.org/licenses/by-nc/4.0/>).

**How to cite this article:** Gireesha B.J., Anitha L. Impact of Shape Dependent Ternary Hybrid Nanoliquid Flow through a Microchannel with Quadratic Thermal Radiation: Irreversibility Analysis, *J. Appl. Comput. Mech.*, xx(x), 2024, 1–13. <https://doi.org/10.22055/jacm.2024.45695.4399>

**Publisher’s Note** Shahid Chamran University of Ahvaz remains neutral with regard to jurisdictional claims in published maps and institutional affiliations.

